

# Particle yields in heavy ion collisions and the influence of strong magnetic fields

---

**M.G. de Paoli and D.P. Menezes**

*Depto de Física - CFM - Universidade Federal de Santa Catarina  
Florianópolis - SC - CP. 476 - CEP 88.040 - 900 - Brazil*

*E-mail:* [marcelodepaoli@gmail.com](mailto:marcelodepaoli@gmail.com), [debora.p.m@ufsc.br](mailto:debora.p.m@ufsc.br)

ABSTRACT: It is expected that the magnetic field in the surface of magnetars do not exceed  $10^{15}$  G. However, in heavy ion collisions, this value is expected to be much higher. We investigate the effects of a magnetic fields varying from  $10^{18}$ , to  $10^{20}$  G in strange matter (composed of  $u$ ,  $d$  and  $s$  quarks). We model matter as a free gas of baryons and mesons under the influence of an external magnetic field. We study the effects of such strong fields through a  $\chi^2$  fit to some data sets of the STAR experiment. For this purpose we solve the Dirac, Rarita-Schwinger, Klein-Gordon and Proca equations subject to magnetic fields in order to obtain the energy expressions and the degeneracy for spin 1/2, spin 3/2, spin 0 and spin 1 particles, respectively. Our results show that a field of the order of  $10^{19}$  G produces an improved fitting to the experimental data as compared to the calculations without magnetic field.

---

## Contents

<b>1</b>	<b>Introduction</b>	<b>1</b>
<b>2</b>	<b>Formalism</b>	<b>2</b>
2.1	Spin 1/2 Baryons	3
2.2	Spin 3/2 Baryons	4
2.3	Spin 0 Mesons	4
2.4	Spin 1 Mesons	5
2.5	Thermodynamics	5
2.6	Chemical Potential	7
<b>3</b>	<b>Results and Discussions</b>	<b>7</b>

---

## 1 Introduction

According to Quantum Chromodynamics, the quark-gluon plasma (QGP) phase refers to matter where quarks and gluons are believed to be deconfined and it probably takes place at temperatures of the order of 150 to 170 MeV. In large colliders around the world (RHIC/BNL, ALICE/CERN, GSI, etc), physicists are trying to find a QGP signature looking at non-central heavy ion collisions.

Possible experiments towards this search are Au-Au collisions at RHIC/BNL and Pb-Pb collisions at SPS/CERN, where the hadron abundances and particle ratios are used in order to determine the temperature and baryonic chemical potential of the possibly present hadronic matter-QGP phase transition.

In previous papers a statistical model under chemical equilibration was used to calculate particle yields [1, 2] and in these works the densities of particles were obtained from free Fermi and Boson gas approximations, where the interaction among the baryons and mesons were neglected. More recently, relativistic nuclear models have been tested in the high temperature regime produced in these heavy ion collisions. In [3, 4] different versions of Walecka-type relativistic models [5] were used to calculate the Au-Au collision particle yields at RHIC/BNL and in [6] the quark-meson-coupling model [7–9] was used to calculate this reaction results and also Pb-Pb collision particle ratios at SPS/CERN. In all cases 18 baryons, pions, kaons,  $\rho$ 's and  $K^*$ s were incorporated in the calculations and a fit based on the minimum value of the quadratic deviation was implemented in order to obtain the temperature and chemical potential for each model, according to a prescription given in [1]. For Au-Au collision (RHIC) these numbers lie in the range  $132 < T < 169$  MeV and  $30.5 < \mu_B < 62.8$  MeV and for Pb-Pb collision (SPS),  $99 < T < 156.1$  MeV and  $167.5 < \mu_B < 411$  MeV.

On the other hand, the magnetic fields involved in heavy-ion collisions [10–12] can reach intensities even higher than the ones considered in magnetars [13, 14]. As suggested in [10–12] and [15–17] it is interesting to investigate fields of the order of  $eB = 5 - 30m_\pi^2$  (corresponding to  $1.7 \times 10^{19} - 10^{20}$  Gauss) and temperatures varying from  $T = 120 - 200$  MeV related to heavy ion collisions. In fact, the densities related to the chemical potentials obtained within the relativistic models framework, in all cases, are very low (of the order of  $10^{-3} \text{ fm}^{-3}$ ). At these densities the nuclear interactions are indeed very small and this fact made us reconsider the possibility of free Fermi and Boson gases, but now under the influence of strong magnetic fields.

In a recent paper [18], the author studies the synchrotron radiation of gluons by fast quarks in strong magnetic fields produced in heavy ion collisions and shows that a strong polarization of quarks and leptons with respect to the direction of the magnetic field is expected. The polarization of quarks seems to be washed out during the fragmentation but this is not the case of the leptons. The observation of lepton polarization asymmetry could be a proof of the existence of the magnetic field, which may last for  $1 - 2 \text{ fm}/c$ . This slowly varying magnetic field could leave its signature in the particle yields.

The purpose of the analysis we present in this paper is to check if the inclusion of strong magnetic fields can improve the fitting of experimental results. We start from the simplest possible calculation, assuming that the magnetic field is homogeneous, constant and time-independent. We are aware that it is not the case, as shown in [19, 20], where the shape of the magnetic field presents a special non-trivial pattern. Moreover, from the calculations performed in these references, one can see that after averaging over many events one is left with just of the components of the magnetic field. Nevertheless, the event-by-event fluctuation of the position of charged particles can induce another component of the magnetic field (perpendicular to the remaining one in the average calculation) and also an electric field, which is quite strong at low impact parameters. While the magnetic field remains quite high in peripheral collisions, the opposite happens with the electric field. To make our first analysis as simple as possible, we shall restrict ourselves to data at centralities of the order of 80%, i.e., high values of the impact parameter  $b \simeq 11 - 13 \text{ fm}$ , where we are more comfortable to disregard the electric field effects.

In the present paper we briefly revisit the formalism necessary for the calculation of particle densities subject to magnetic fields and the expressions used to implement a  $\chi^2$  fit to the experimental results.

## 2 Formalism

We model matter as a free gas of baryons and mesons under the influence of a constant magnetic field. We consider only normal and strange matter, i.e., the baryons and mesons constituted by  $u$ ,  $d$  and  $s$  quarks: the baryon octet (spin 1/2 baryons), the baryon decuplet (spin 3/2 baryons), the pseudoscalar meson nonet (spin 0 mesons) and the vector meson nonet (spin 1 mesons), which leaves us with a total of 54 particles (18 baryons, 18 antibaryons and 18 mesons).

We utilize natural units ( $\hbar = c = 1$ ) and define  $\epsilon_0 = \mu_0 = 1$ . From the relation  $\alpha = \frac{e^2}{4\pi\epsilon_0\hbar c}$  we obtain that the electron charge is  $e = \sqrt{4\pi\alpha}$ , where  $\alpha = \frac{1}{137}$  is the fine structure constant. The natural units with the electron charge in that form is known as Heaviside-Lorentz units [21].

In this work, the magnetic field is introduced through minimal coupling, so the derivatives become

$$\partial_\mu \rightarrow D_\mu = \partial_\mu + iqA_\mu. \quad (2.1)$$

We write the charge as  $q = \epsilon_q|q|$ , where  $\epsilon_q = +(-)$  corresponds to a particle with positive (negative) charge, and assume the gauge

$$A_\mu = \delta_{\mu 2}x_1B \quad \rightarrow \quad A_0 = 0 \quad \text{and} \quad \vec{A} = (0, x_1B, 0), \quad (2.2)$$

so,

$$\vec{\nabla} \cdot \vec{A} = 0 \quad \text{and} \quad \vec{\nabla} \times \vec{A} = B\hat{e}_3, \quad (2.3)$$

and the derivatives

$$D_\mu = \partial_\mu - i\epsilon_q|q|Bx_1\delta_{\mu 2}. \quad (2.4)$$

We search for solutions of the fields  $\psi$  in the form

$$\psi_\alpha^{(\epsilon)} = \begin{cases} C_\alpha^{(\epsilon)} e^{-i\epsilon Et + i\epsilon \vec{p} \cdot \vec{x}} & (q = 0) \\ f_\alpha^{(\epsilon)}(x_1) e^{-i\epsilon Et + i\epsilon p_2 x_2 + i\epsilon p_3 x_3} & (q \neq 0) \end{cases}, \quad (2.5)$$

where  $\psi_\alpha$  are the components of the field  $\psi$  and  $\epsilon = +(-)$  corresponds to the states of positive (negative) energy.

For the spin 1/2 baryons (Dirac field)  $\psi$  has 4 components, for the spin 3/2 baryons (Rarita-Schwinger field)  $\psi_\mu$  has 16 components, for the spin 0 mesons (Klein-Gordon field)  $\psi$  has just one component, and for the spin 1 mesons (Proca field)  $\psi_\mu$  has 4 components.

Due to the use of statistical methods to deal with the system under consideration, we do not need the complete expression for  $\psi$ , but just the form of the energy  $E$  for each one of the fields and the degeneracy of the energy levels  $\gamma$ .

## 2.1 Spin 1/2 Baryons

The baryons with spin 1/2 are described by the Dirac Lagrangian density [22]

$$\mathcal{L}^D = \bar{\psi}(i\gamma^\mu D_\mu - m)\psi, \quad (2.6)$$

which (after we apply the Euler-Lagrange equation) lead us to the equation of motion

$$(i\gamma^\mu D_\mu - m)\psi = 0. \quad (2.7)$$

where  $\gamma^\mu$  are the Dirac matrices.

The solution of the equation of motion gives

$$E = \begin{cases} \sqrt{\vec{p}^2 + m^2} & (q = 0) \\ \sqrt{p_3^2 + m^2 + 2\nu|q|B} & (q \neq 0) \end{cases}, \quad (2.8)$$

where  $\nu$  runs over the possible Landau Levels and the degeneracy for the energy states are given by:

$$\gamma = \begin{cases} 2 & (q = 0) \\ 2 - \delta_{\nu 0} & (q \neq 0) \end{cases}. \quad (2.9)$$

## 2.2 Spin 3/2 Baryons

The baryons with spin 3/2 are described by the Rarita-Schwinger Lagrangian density [23, 24]

$$\mathcal{L}^{RS} = -\frac{1}{2}\bar{\psi}_\mu(\epsilon^{\mu\nu\rho\sigma}\gamma_5\gamma_\nu D_\rho + im\sigma^{\mu\sigma})\psi_\sigma, \quad (2.10)$$

where  $\gamma^5 = i\gamma^0\gamma^1\gamma^2\gamma^3$  and  $\sigma^{\mu\nu} = \frac{i}{2}[\gamma^\mu, \gamma^\nu]$ .

The equation of motion reads

$$(i\gamma^\mu D_\mu - m)\psi_\nu = 0 \quad \text{with} \quad \gamma^\mu\psi_\mu = 0 \quad \text{and} \quad D^\mu\psi_\mu = 0. \quad (2.11)$$

The solution of the Rarita-Schwinger equation is not trivial and poses non-causality problems. To obtain the degeneracy of the energy states, we follow the prescription used in [22], which is given in detail for the Rarita-Schwinger equation in [25]. Observing the equation of motion one can see that each component of  $\psi_\mu$  obeys a Dirac type equation, so the energy must have the form

$$E = \begin{cases} \sqrt{\vec{p}^2 + m^2} & (q = 0) \\ \sqrt{p_3^2 + m^2 + 2\nu|q|B} & (q \neq 0) \end{cases}. \quad (2.12)$$

Besides that,  $\psi_\mu$  has 4 components, but, two equations are constrained, which means that only 2 components of  $\psi_\mu$  are really independent. So,  $\psi_\mu$  have 2 polarizations, but, (because of the Dirac equation solution) each polarization are double degenerate. In the presence of a magnetic field there is another constraint for the  $\nu = 0$  and  $\nu = 1$  energy levels, which leads to the following degeneracy for the energy states

$$\gamma = \begin{cases} 4 & (q = 0) \\ 4 - 2\delta_{\nu 0} - \delta_{\nu 1} & (q \neq 0) \end{cases}. \quad (2.13)$$

## 2.3 Spin 0 Mesons

The mesons with spin 0 are described by the Klein-Gordon Lagrangian density [26]

$$\mathcal{L}^{KG} = D^\mu\psi^* D_\mu\psi - m^2\psi^*\psi, \quad (2.14)$$

whose equation of motion is given by

$$(D^\mu D_\mu + m^2)\psi = 0, \quad (2.15)$$

with the energy satisfying the relation:

$$E = \begin{cases} \sqrt{\vec{p}^2 + m^2} & (q = 0) \\ \sqrt{p_3^2 + m^2 + (2\nu + 1)|q|B} & (q \neq 0) \end{cases}. \quad (2.16)$$

## 2.4 Spin 1 Mesons

The mesons with spin 1 are described by the Proca Lagrangian density [27]

$$\mathcal{L}^P = \frac{1}{2}(D^\mu\psi^{\nu*} - D^\nu\psi^{\mu*})(D_\mu\psi_\nu - D_\nu\psi_\mu) - m^2\psi^{\nu*}\psi_\nu. \quad (2.17)$$

The equation of motion is

$$(D^\mu D_\mu + m^2)\psi_\nu = 0 \quad \text{with} \quad D_\mu\psi^\mu = 0. \quad (2.18)$$

Each component of  $\psi_\mu$  obey a Klein-Gordon type equation, so that the energy states are

$$E = \begin{cases} \sqrt{p^2 + m^2} & (q = 0) \\ \sqrt{p_3^2 + m^2 + (2\nu + 1)|q|B} & (q \neq 0) \end{cases}, \quad (2.19)$$

$\psi_\mu$  has 4 components, but, one of the equations is a compressed constraint equation, which means that only 3 components of  $\psi_\mu$  are independent. So, each energy state have 3 polarizations in the case with zero charge (or without magnetic field). If the charge is different from zero (and we have the presence of an external magnetic field) there is an additional constraint for the  $\nu = 0$  energy level, which leads to the following degeneracy for the energy states

$$\gamma = \begin{cases} 3 & (q = 0) \\ 3 - \delta_{\nu 0} & (q \neq 0) \end{cases}. \quad (2.20)$$

## 2.5 Thermodynamics

Using the Grand Canonical formalism we obtain that the particle densities for the baryons are

$$\rho_b = \begin{cases} \gamma_b \frac{1}{2\pi^2} \int_0^\infty f(E_b - \mu_b) p^2 dp & (q = 0) \\ \sum_{\nu=0}^\infty \gamma_b \frac{|q_b|B}{2\pi^2} \int_0^\infty f(E_b - \mu_b) dp & (q \neq 0) \end{cases}, \quad (2.21)$$

for the antibaryons are

$$\rho_{ab} = \begin{cases} \gamma_b \frac{1}{2\pi^2} \int_0^\infty f(E_b + \mu_b) p^2 dp & (q = 0) \\ \sum_{\nu=0}^\infty \gamma_b \frac{|q_b|B}{2\pi^2} \int_0^\infty f(E_b + \mu_b) dp & (q \neq 0) \end{cases}, \quad (2.22)$$

and for the mesons are

$$\rho_m = \begin{cases} \gamma_m \frac{1}{2\pi^2} \int_0^\infty b(E_m - \mu_m) p^2 dp & (q = 0) \\ \sum_{\nu=0}^\infty \gamma_m \frac{|q_m|B}{2\pi^2} \int_0^\infty b(E_m - \mu_m) dp & (q \neq 0) \end{cases}, \quad (2.23)$$

with  $f(x) = (e^{x/T} + 1)^{-1}$  and  $b(x) = (e^{x/T} - 1)^{-1}$ .

The total baryonic particle density is

$$\rho_B = \sum_b (\rho_b - \rho_{ab}), \quad (2.24)$$

and the total mesonic density is

$$\rho_M = \sum_m \rho_m. \quad (2.25)$$

The energy density is given by the sum of the energy densities of each particle, so

$$\epsilon = \sum_b (\epsilon_b + \epsilon_{ab}) + \sum_m \epsilon_m, \quad (2.26)$$

with

$$\epsilon_b = \begin{cases} \gamma_b \frac{1}{2\pi^2} \int_0^\infty E_b f(E_b - \mu_b) p^2 dp & (q = 0) \\ \sum_{\nu=0}^\infty \gamma_b \frac{|q_b| B}{2\pi^2} \int_0^\infty E_b f(E_b - \mu_b) dp & (q \neq 0) \end{cases}, \quad (2.27)$$

$$\epsilon_{ab} = \begin{cases} \gamma_b \frac{1}{2\pi^2} \int_0^\infty E_b f(E_b + \mu_b) p^2 dp & (q = 0) \\ \sum_{\nu=0}^\infty \gamma_b \frac{|q_b| B}{2\pi^2} \int_0^\infty E_b f(E_b + \mu_b) dp & (q \neq 0) \end{cases}, \quad (2.28)$$

$$\epsilon_m = \begin{cases} \gamma_m \frac{1}{2\pi^2} \int_0^\infty E_m b(E_m - \mu_m) p^2 dp & (q = 0) \\ \sum_{\nu=0}^\infty \gamma_m \frac{|q_m| B}{2\pi^2} \int_0^\infty E_m b(E_m - \mu_m) dp & (q \neq 0) \end{cases}, \quad (2.29)$$

in the same way the pressure is given by

$$P = \sum_b (P_b + P_{ab}) + \sum_m P_m, \quad (2.30)$$

with

$$P_b = \begin{cases} \gamma_b \frac{1}{6\pi^2} \int_0^\infty \frac{1}{E_b} f(E_b - \mu_b) p^4 dp & (q = 0) \\ \sum_{\nu=0}^\infty \gamma_b \frac{|q_b| B}{2\pi^2} \int_0^\infty \frac{1}{E_b} f(E_b - \mu_b) p^2 dp & (q \neq 0) \end{cases}, \quad (2.31)$$

$$P_{ab} = \begin{cases} \gamma_b \frac{1}{6\pi^2} \int_0^\infty \frac{1}{E_b} f(E_b + \mu_b) p^4 dp & (q = 0) \\ \sum_{\nu=0}^\infty \gamma_b \frac{|q_b| B}{2\pi^2} \int_0^\infty \frac{1}{E_b} f(E_b + \mu_b) p^2 dp & (q \neq 0) \end{cases}, \quad (2.32)$$

$$P_m = \begin{cases} \gamma_m \frac{1}{6\pi^2} \int_0^\infty \frac{1}{E_m} b(E_m - \mu_m) p^4 dp & (q = 0) \\ \sum_{\nu=0}^\infty \gamma_m \frac{|q_m| B}{2\pi^2} \int_0^\infty \frac{1}{E_m} b(E_m - \mu_m) p^2 dp & (q \neq 0) \end{cases}, \quad (2.33)$$

the entropy density can be found through

$$s = \epsilon + P - \sum_b \mu_b (\rho_b - \rho_{ab}) - \sum_m \mu_m \rho_m. \quad (2.34)$$

## 2.6 Chemical Potential

The hadron chemical potential is

$$\mu_h = B_h \mu_B + I_{3h} \mu_{I_3} + S_h \mu_S, \quad (2.35)$$

where  $B_h$ ,  $I_{3h}$  and  $S_h$ , are respectively the baryonic number, the third isospin component and the strangeness of the particle  $h$ . The baryonic chemical potential  $\mu_B$  is a free parameter of the system (the other is the temperature  $T$ ). The chemical potential of isospin  $\mu_{I_3}$  and strangeness  $\mu_S$  are determined through their respective conservation laws.

We impose the local conservation of the baryonic number, isospin and strangeness. This imposition leads to the following equations

$$\sum_h B_h \rho_h = \frac{N_B}{V}, \quad \sum_h I_{3h} \rho_h = \frac{I_3}{V}, \quad \sum_h S_h \rho_h = \frac{S}{V}, \quad (2.36)$$

where  $N_B$  is the total baryonic number,  $I_3$  is the total isospin,  $S$  is the total strangeness of the system and  $V$  are the volume occupied by the system. The charge conservation is automatically achieved through the other three conservation laws.

The baryonic number of an Au atom is  $N_B = (N + Z) = 79 + 118 = 197$ , the isospin is  $I_3 = (Z - N)/2 = 19.5$  and for the deuteron ( $d$ ) we have that  $N_B = 1 + 1 = 2$  and  $I_3 = 0$ . Hence, assuming that the total strangeness of the system is zero, we write the following table for the conserved quantities:

- Au+Au Collision,  $N_B = 394$ ,  $I_3 = -39$ ,  $S = 0$ .
- $d$ +Au Collision,  $N_B = 199$ ,  $I_3 = -19.5$ ,  $S = 0$ .

At this point it is important to emphasize some of the drawbacks of our simple calculation. As shown in [28], the magnetic field should depend on the charges of the colliding nuclei and the number of participants should vary for different centralities. These constraints were not taken into account directly in our calculations. All the information we use as input come from the experimental particle yields and the magnetic field is modified until the best fitting is encountered. The number of different participants is reflected only in the resulting radii.

## 3 Results and Discussions

We have implemented a  $\chi^2$  fit in order to obtain the temperature and chemical potential. The particle properties (spin, mass, baryonic number, isospin and strangeness) were taken from the *Particle Data Group* [29].



In tables 1, 2, 3 and 4 we show our results corresponding to the temperature and chemical potential that give the minimum value for the quadratic deviation  $\chi^2$ :

$$\chi^2 = \sum_i \frac{(\mathcal{R}_i^{exp} - \mathcal{R}_i^{theo})^2}{\sigma_i^2}, \quad (3.1)$$

where  $\mathcal{R}_i^{exp}$  and  $\mathcal{R}_i^{theo}$  are the  $i^{th}$  particle ratio given experimentally and theoretically, and  $\sigma_i$  represents the errors in the experimental data points.

To make clear the improvement in the data fitting by the addition of the magnetic field, we calculate the relative percent deviation ( $\Delta\%$ ) with respect to the experimental values for  $B = 0$  and the best  $B \neq 0$  (the bold columns in the tables) through the equation

$$\Delta\% = \left| \frac{\mathcal{R}^{theo} - \mathcal{R}^{exp}}{\mathcal{R}^{exp}} \right| \cdot 100\%, \quad (3.2)$$

and show these values in parenthesis in all the tables.

For the simulations our code deals with 5 unknowns ( $\mu_B, \mu_{I3}, \mu_S, T, V$ ) and 3 constrained equations. We run over the values of  $\mu_B$  and  $T$  (the free parameters) in order to find the smallest  $\chi^2$ . Our results are given next.

In tables 1, 2, 3 and 4,  $B$  is the magnetic field,  $T$  is the temperature,  $\mu_B$  is the baryonic chemical potential,  $\chi^2$  is quadratic deviation,  $\mu_{I3}$  is the isospin chemical potential,  $\mu_S$  is the strangeness chemical potential,  $R$  is the radius of the "fire-ball",  $\rho_B = \sum_b(\rho_b - \rho_{ab})$  is the usual baryonic density,  $\rho_\Delta = \rho_{\Delta^{++}} - \rho_{\bar{\Delta}^{++}} + \rho_{\Delta^+} - \rho_{\bar{\Delta}^+} + \rho_{\Delta^0} - \rho_{\bar{\Delta}^0} + \rho_{\Delta^-} - \rho_{\bar{\Delta}^-}$  is delta baryon density,  $\rho_M = \sum_m \rho_m$  is the meson density,  $\rho_\pi = \rho_{\pi^0} + \rho_{\pi^+} + \rho_{\pi^-}$  is the pion density,  $\epsilon$  is the energy density,  $P$  is the pressure,  $s$  is the entropy density and  $ndf$  is the number of degrees of freedom. For  $B = 0$ ,  $ndf = 5$  (7 experimental values minus 2 free parameters,  $T$  and  $\mu$ ), for  $B \neq 0$ ,  $ndf = 4$  (7 experimental values minus 3 free parameters,  $T$ ,  $\mu$  and  $B$ ).  $\pi^-/\pi^+$ ,  $K^-/K^+$ ,  $\bar{p}/p$ ,  $K^-/\pi^-$ ,  $K^+/\pi^+$  and  $p/\pi^+$  are the theoretical (first 7 columns) and experimental (last column) particle ratios [30]. The temperatures and baryonic chemical potentials obtained from the statistical model in [30] are also given in the last columns of all tables.

In figs. 1-a/b, 2-a/b, 3-a/b and 4-a/b we plot the experimental and theoretical ratios for  $B = 0$  and the best  $B \neq 0$ . In figs. 1-c, 2-c, 3-c and 4-c we show the  $\chi^2$  behavior for  $B = 0$  and for the best  $B \neq 0$ . In figs. 1-d, 2-d, 3-d and 4-d we show the  $\chi^2$  behavior for the different magnetic fields. One can notice that the best fitting is generally obtained for magnetic fields around  $6 m_\pi^2$ , a little higher than what is expected for RHIC collisions ( $5 m_\pi^2$ ).

Our results show that, even for the free Fermi and Boson gas models, a strong magnetic field plays an important role. The inclusion of the magnetic field improves the data fit up to a field of the order of  $B = 10^{19}$  G. For stronger magnetic fields, it becomes worse again. This behavior is easily observed in tables 1 to 4 and in figs.1-d to 4-d. It is worth pointing out how the "fireball" radius  $R$  and the total density  $\rho$  vary with the magnetic field in a systematic way:  $R$  and  $\rho$  practically do not change between  $B = 0$  and  $B = 10^{18}$  G, but when the field increases even further, the density increases and the radius decreases. This

behavior is common to all collision cases studied. This huge jump in the density explains why the ratios get worse for a magnetic field of the order of  $B = 10^{20}$  G, for which the densities are much higher than what is expected in a heavy ion collision.

Our model gives a good description for the particle/antiparticle ratios, but fails to describe the relation between baryons and mesons. This occurs because our model produces too many mesons (especially pions) as shown explicitly in the particle densities. In all collision types our model presents a baryon density ( $\rho_B$ ) with more than 30% of  $\Delta$  baryons and a meson density ( $\rho_M$ ) with more than 60% of  $\pi$  ( $\rho_\pi$ ). The relative percent deviations in the particle yields show clearly that some results improve considerably when the magnetic field is considered, while others remain unaltered or even get slightly worse. However, our figures also show that the behavior of the  $\chi^2$  changes drastically with the addition of the magnetic field and that the temperature and chemical potentials calculated with the statistical model lie within the  $3 - \sigma$  confidence ellipse obtained for the best  $\chi^2$  in some cases, but they are always outside the confidence ellipses obtained with zero magnetic field.

We would like to comment that when we first started these calculations, we were not aware of references [19, 20] and we used data obtained for low centralities, i.e., low impact parameters. In that case, the minimum  $\chi^2$  was generally smaller than the ones shown in this work and we believe this was so because of the larger error bars accompanying data at low centralities.

Further improvements on the presented calculations are under investigation, namely, the inclusion of electric fields at low impact parameters and the variation of both electric and magnetic fields with the number of participants in the collisions. Moreover, we are working on the inclusion of the anomalous magnetic moments and in the description of pion-pion interactions. We next intend to repeat these calculations for the ALICE/LHC data for the future Au+Au runs with all these improvements, so that our results become more realistic.

## Acknowledgments

This work was partially supported by CNPq, CAPES and FAPESC (Brazil). We thank very fruitful discussions with Dr. Celso Camargo de Barros and Dr. Sidney dos Santos Avancini.

## References

- [1] P. Braun-Munzinger, I. Heppe and J. Stachel, *Chemical equilibration in Pb-Pb collisions at the SPS* Phys. Lett. B **465** (1999), 15-20 [nucl-th/9903010].
- [2] P. Braun-Munzinger, D. Magestro, K. Redlich and J. Stachel, *Hadron production in Au-Au collisions at RHIC*, Phys. Lett. B **518** (2001), 41-46 [hep-ph/0105229].
- [3] D. P. Menezes, C. Providência, M. Chiapparini, M. E. Bracco, A. Delfino, and M. Malheiro, *Constraining relativistic models through heavy ion collisions*, Phys. Rev. C **76** (2007), 064902 [hep-ph/0708.3380].

- [4] M. Chiapparini, M. E. Bracco, A. Delfino, M. Malheiro, D. P. Menezes and C. Providência, *Hadron production in non linear relativistic mean field models* Nucl. Phys. A **826** (2009), 178-189 [hep-ph/0711.3631].
- [5] B. Serot and J. D. Walecka, *Advances in Nuclear Physics* **16**, Plenum-Press (1986).
- [6] P. K. Panda, D.P. Menezes and C. Providência, *Particle production within the quark meson coupling model*, Phys. Rev. C **80** (2009), 014905 [nucl-th/0904.3837].
- [7] P. A. M. Guichon, *A possible quark mechanism for the saturation of nuclear matter*, Phys. Lett. B **200** (1988), 235-240.
- [8] K. Saito and A. W. Thomas, *A quark-meson coupling model for nuclear and neutron matter*, Phys. Lett. B **327** (1994), 9-16 [nucl-th/9403015].
- [9] K. Tsushima, K. Saito, A.W. Thomas and S.W. Wright, *In-medium kaon and antikaon properties in the quark-meson coupling model*, Phys. Lett. B **429** (1998), 239-246 [nucl-th/9712044].
- [10] K. Fukushima, D. E. Kharzeev and H. J. Warringa, *The chiral magnetic effect* Phys. Rev. D **78** (2008), 074033 [hep-ph/0808.3382].
- [11] D. E. Kharzeev and H. J. Warringa, *Chiral magnetic conductivity*, Phys. Rev. D **80** (2009), 034028 [hep-ph/0907.5007].
- [12] D. E. Kharzeev, *Chern-Simons current and local parity violation in hot QCD matter*, Nucl. Phys. A **830** (2009), 543c-546c, [hep-ph/0908.0314].
- [13] R. Duncan and C. Thompson, *Formation of very strongly magnetized neutron stars - Implications for gamma-ray bursts*, Astrophysical Journal, Part 2 - Letters **392** (1992), L9-L13.
- [14] C. Kouveliotou et al, *An X-ray pulsar with a superstrong magnetic field in the soft  $\gamma$ -ray repeater SGR1806-20*, Nature **393** (1998), 235-237.
- [15] E. S. Fraga and A. J. Mizher, *Chiral transition in a strong magnetic background*, Phys. Rev. D **78** (2008), 025016 [hep-ph/0804.1452].
- [16] E. S. Fraga and A. J. Mizher, *Chiral symmetry restoration and strong CP violation in a strong magnetic background*, PoS **37** (2009) [hep-ph/0910.4525].
- [17] E. S. Fraga, M. N. Chernodub and A. J. Mizher, *Phase diagram of hot QCD in an external magnetic field: possible splitting of deconfinement and chiral transitions*, Phys. Rev. D **82** (2010), 105016 [hep-ph/1004.2712].
- [18] K. Tuchin, *Synchrotron radiation by fast fermions in heavy-ion collisions*, Phys. Rev. C **82**, 034904 (2010) [Erratum *ibid* **83** (2011), 039903] [nucl-th/1006.3051].
- [19] A. Bzdak, V. Skokov, *Event-by-event fluctuations of magnetic and electric fields in heavy-ion collisions*, Phys. Lett. B **710** (2012), 171-174 [hep-ph/1111.1949].
- [20] W-T. Deng and X-G Huang, *Event-by-event generation of electromagnetic fields in heavy-ion collisions*, Phys. Rev. C **85** (2012), 044907 [nucl-th/1201.5108v2].
- [21] J. D. Jackson, *Classical Electrodynamics*, 3th Edition, John Wiley & Sons, Inc., 1999.
- [22] D. B. Melrose and A. J. Parle, *Quantum electrodynamics in strong magnetic fields: I Electron*, Aus. J. Phys. 1983, **36**, 755-774.

- [23] W. Rarita and J. Schwinger, *On a theory of particles with half-integral spin*, Phys. Rev. **60**, 61 (1941).
- [24] S. Weinberg, *The Quantum Theory of fields, Vol. III, Supersymmetry*, Cambridge University Press, 2000.
- [25] M.G. de Paoli, L.B. Castro, D.P. Menezes and C.C. Barros Jr., *The Rarita-Schwinger particles under the influence of strong magnetic fields* [math-ph/1207.4063].
- [26] W. Greiner and J. Reinhardt, *Field Quantization*, Springer, 1996.
- [27] I. A. Obukhov, V. K. Peres-Fernandes, I. M. Ternov and V. R. Khalilov, Moscow State University. *Charged vector particles in a magnetic field*, Teoret. Mat. Fiz., **55**:3 (1983), 335-348.
- [28] D. E. Kharzeev, L.D. McLerran and H. J. Warringa, *The effects of topological charge change in heavy ion collisions: "Event by event P and CP violation"*, Nucl. Phys. A **803** (2008), 227253 [hep-ph/0711.0950].
- [29] K. Nakamura, *et al.* (Particle Data Group), *Review of particle physics*, J. Phys. G **37** (2010), 075021.
- [30] B. I. Abelev, *et al.* (STAR Collaboration), *Systematic measurements of identified particle spectra in pp, d+Au, and Au+Au collisions at the STAR detector*, Phys. Rev. C **79** (2009), 034909.

$B$ ( $\times 10^{19}$ G)	0	0.1	0.5	1	<b>2</b>	5	10	STAR/RHIC[30]
$eB$ ( $m_\pi^2$ )	0	0.3	1.5	3	<b>6</b>	15	30	
$\pi^-/\pi^+$ ( $\Delta\%$ )	1.000 (0.30%)	1.000	1.000	1.000	<b>1.000 (0.30%)</b>	1.000	1.000	1.003 $\pm$ 0.044
$K^-/K^+$	0.993 (1.23%)	0.993	0.986	0.980	<b>0.971 (0.99%)</b>	0.966	0.939	0.981 $\pm$ 0.049
$\bar{p}/p$	0.842 (0.13%)	0.843	0.834	0.839	<b>0.837 (0.69%)</b>	0.836	0.776	0.843 $\pm$ 0.048
$K^-/\pi^-$	0.169 (32.7%)	0.169	0.175	0.177	<b>0.178 (40.1%)</b>	0.182	0.218	0.127 $\pm$ 0.010
$\bar{p}/\pi^-$	0.019 (77.8%)	0.019	0.026	0.033	<b>0.037 (55.7%)</b>	0.036	0.046	0.084 $\pm$ 0.007
$K^+/\pi^+$	0.170 (30.5%)	0.170	0.177	0.181	<b>0.183 (40.9%)</b>	0.189	0.232	0.130 $\pm$ 0.011
$p/\pi^+$	0.022 (77.9%)	0.023	0.031	0.039	<b>0.044 (55.6%)</b>	0.043	0.059	0.100 $\pm$ 0.013
$T$ (MeV)	124	125	138	152	<b>170</b>	194	199	157.9 $\pm$ 3.9
$\mu_B$ (MeV)	11	11	13	14	<b>16</b>	19	20	14.1 $\pm$ 4.2
$\mu_S$ (MeV)	0.758	0.787	1.43	2.15	<b>3.28</b>	4.82	5.08	
$\mu_{I3}$ (MeV)	-0.653	-0.660	-0.949	-1.22	<b>-1.76</b>	-3.24	-5.00	
$\chi^2/ndf$	42.5	52.5	46.0	39.8	<b>35.6</b>	39.7	47.9	
$R$ (fm)	66.2	64.6	45.5	34.0	<b>24.5</b>	16.8	14.8	
$\rho_B$ ( $\times 10^{-2}$ fm $^{-3}$ )	0.0325	0.0349	0.100	0.239	<b>0.643</b>	2.00	2.91	
$\rho_\Delta$ ( $\times 10^{-2}$ fm $^{-3}$ )	0.00813	0.00878	0.0276	0.0717	<b>0.211</b>	0.732	1.14	
$\rho_M$ (fm $^{-3}$ )	0.0918	0.0960	0.167	0.293	<b>0.582</b>	1.51	2.73	
$\rho_\pi$ (fm $^{-3}$ )	0.0636	0.0664	0.109	0.183	<b>0.355</b>	0.942	1.83	
$\epsilon$ (MeV/fm $^3$ )	55.4	58.3	111	212	<b>456</b>	1203	1820	
$P$ (MeV/fm $^3$ )	11.2	11.8	22.6	43.7	<b>97.4</b>	283	490	
$s$ (MeV/fm $^3$ )	0.537	0.561	0.967	1.68	<b>3.26</b>	7.66	11.6	

**Table 1.** Au+Au (70-80%)  $\sqrt{s_{NN}} = 200$  GeV. Results obtained for different values of the magnetic field.

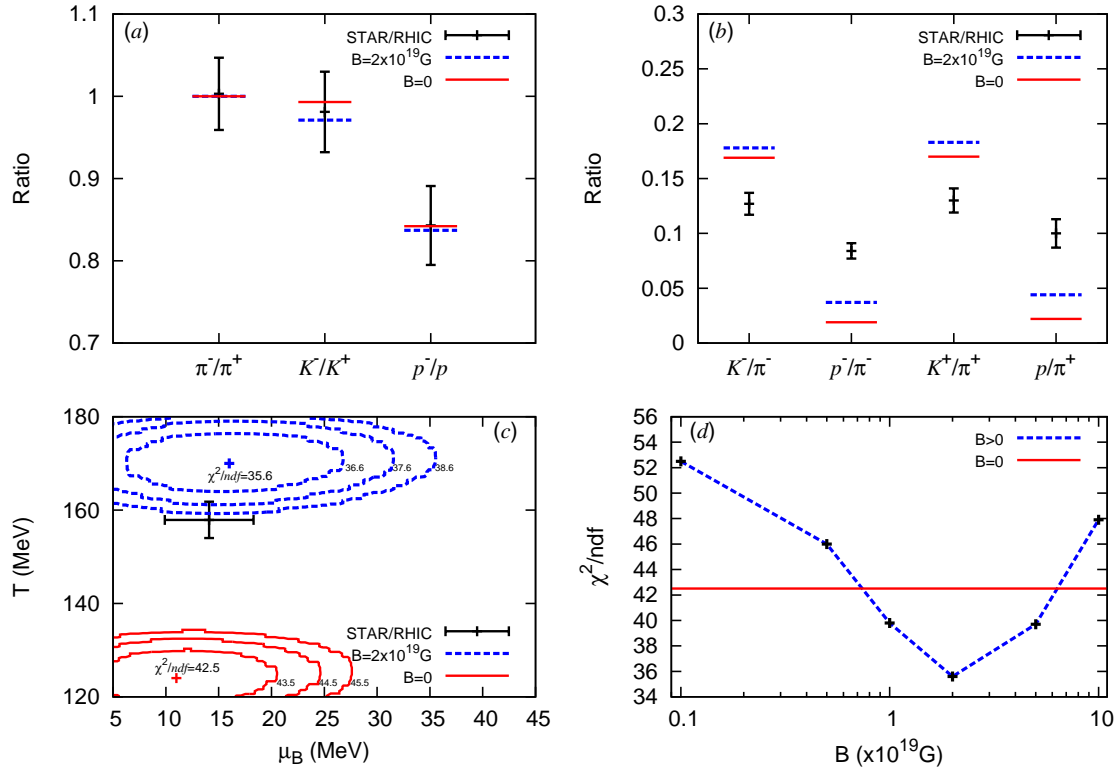


**Figure 1.** Au+Au (70-80%) collision at  $\sqrt{s_{NN}} = 200$  GeV. (a) particle/antiparticle ratios. (b) mixed ratios. (c) and (d)  $\chi^2$  behavior.

$B$ ( $\times 10^{19}$ G)	0	0.1	0.5	1	<b>2</b>	5	10	STAR/RHIC[30]
$eB$ ( $m_\pi^2$ )	0	0.3	1.5	3	<b>6</b>	15	30	
$\pi^-/\pi^+$ ( $\Delta\%$ )	1.000 (0.40%)	1.000	1.000	1.000	<b>1.000 (0.40%)</b>	1.000	1.000	$0.996\pm 0.066$
$K^-/K^+$	0.985 (2.32%)	0.984	0.977	0.967	<b>0.956 (0.71%)</b>	0.947	0.952	$0.963\pm 0.050$
$\bar{p}/p$	0.793 (0.35%)	0.783	0.788	0.787	<b>0.792 (0.25%)</b>	0.794	0.792	$0.790\pm 0.043$
$K^-/\pi^-$	0.196 (40.3%)	0.196	0.195	0.195	<b>0.194 (38.53%)</b>	0.199	0.201	$0.140\pm 0.018$
$\bar{p}/\pi^-$	0.027 (67.6%)	0.027	0.033	0.040	<b>0.045 (44.9%)</b>	0.045	0.036	$0.082\pm 0.010$
$K^+/\pi^+$	0.199 (38.2%)	0.200	0.200	0.202	<b>0.203 (40.9%)</b>	0.210	0.211	$0.144\pm 0.016$
$p/\pi^+$	0.034 (67.4%)	0.035	0.042	0.050	<b>0.057 (44.6%)</b>	0.057	0.046	$0.103\pm 0.012$
$T$ (MeV)	133	134	145	159	<b>178</b>	206	217	$159^{+11}_{-7}$
$\mu_B$ (MeV)	16	17	18	20	<b>22</b>	26	29	$19.9\pm 4.9$
$\mu_S$ (MeV)	1.52	1.67	2.39	3.55	<b>5.07</b>	7.38	8.42	
$\mu_{I3}$ (MeV)	-1.10	-1.18	-1.41	-1.79	<b>-2.41</b>	-4.26	-6.92	
$\chi^2/ndf$	17.2	21.2	17.9	14.8	<b>12.7</b>	14.2	18.1	
$R$ (fm)	47.1	45.2	35.5	26.9	<b>19.8</b>	13.4	11.1	
$\rho_B$ ( $\times 10^{-2}$ fm $^{-3}$ )	0.0899	0.102	0.211	0.486	<b>1.22</b>	3.95	6.92	
$\rho_\Delta$ ( $\times 10^{-2}$ fm $^{-3}$ )	0.0243	0.0273	0.0610	0.151	<b>0.415</b>	1.50	2.82	
$\rho_M$ (fm $^{-3}$ )	0.127	0.132	0.207	0.352	<b>0.693</b>	1.84	3.49	
$\rho_\pi$ (fm $^{-3}$ )	0.0813	0.0845	0.127	0.208	<b>0.398</b>	1.07	2.16	
$\epsilon$ (MeV/fm $^3$ )	86.4	90.6	152	282	<b>608</b>	1704	2863	
$P$ (MeV/fm $^3$ )	17.0	17.8	30.2	56.6	<b>126</b>	385	729	
$s$ (MeV/fm $^3$ )	0.777	0.809	1.26	2.13	<b>4.12</b>	10.1	16.5	

**Table 2.** Au+Au (58-85%) collision at  $\sqrt{s_{NN}} = 130$  GeV. Results obtained for different values of the magnetic field.

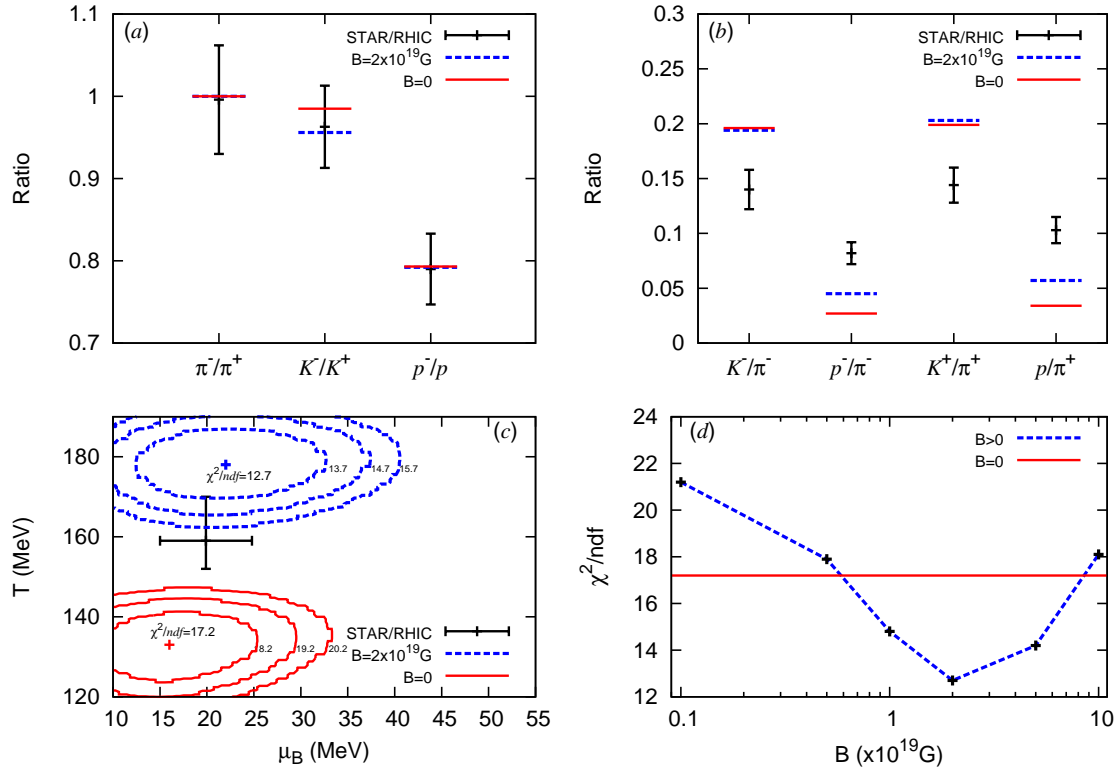


**Figure 2.** Au+Au (58-85%) collision at  $\sqrt{s_{NN}} = 130$  GeV. (a) particle/antiparticle ratios. (b) mixed ratios. (c) and (d)  $\chi^2$  behavior.



$B$ ( $\times 10^{19}$ G)	0	0.1	0.5	1	<b>2</b>	5	10	STAR/RHIC[30]
$eB$ ( $m_\pi^2$ )	0	0.3	1.5	3	<b>6</b>	15	30	
$\pi^-/\pi^+$ ( $\Delta\%$ )	1.000 (1.19%)	1.000	1.000	1.000	<b>1.000 (1.19%)</b>	1.000	1.000	1.012 $\pm$ 0.031
$K^-/K^+$	0.992 (5.97%)	0.991	0.982	0.971	<b>0.958 (2.34%)</b>	0.959	0.972	0.936 $\pm$ 0.036
$\bar{p}/p$	0.621 (0.27%)	0.624	0.623	0.625	<b>0.625 (0.26%)</b>	0.623	0.618	0.623 $\pm$ 0.047
$K^-/\pi^-$	0.128 (17.0%)	0.128	0.130	0.132	<b>0.132 (20.9%)</b>	0.131	0.129	0.109 $\pm$ 0.009
$\bar{p}/\pi^-$	0.008 (87.1%)	0.008	0.011	0.014	<b>0.016 (74.7%)</b>	0.013	0.010	0.063 $\pm$ 0.007
$K^+/\pi^+$	0.129 (8.99%)	0.129	0.133	0.136	<b>0.138 (16.6%)</b>	0.137	0.132	0.118 $\pm$ 0.010
$p/\pi^+$	0.013 (87.1%)	0.013	0.018	0.023	<b>0.026 (74.7%)</b>	0.021	0.016	0.101 $\pm$ 0.013
$T$ (MeV)	111	112	123	135	<b>149</b>	162	193	154 $^{+8}_{-6}$
$\mu_B$ (MeV)	27	27	30	33	<b>37</b>	42	45	37.7 $\pm$ 6.5
$\mu_S$ (MeV)	1.04	1.09	1.97	3.24	<b>5.06</b>	6.93	7.85	
$\mu_{I3}$ (MeV)	-1.17	-1.20	-1.75	-2.49	<b>-3.83</b>	-7.28	-11.3	
$\chi^2/ndf$	23.0	28.5	26.0	23.7	<b>22.4</b>	24.9	27.5	
$R$ (fm)	70.4	68.4	48.6	35.4	<b>25.7</b>	19.3	17.3	
$\rho_B$ ( $\times 10^{-2}$ fm $^{-3}$ )	0.0269	0.0295	0.0821	0.212	<b>0.552</b>	1.31	1.81	
$\rho_\Delta$ ( $\times 10^{-2}$ fm $^{-3}$ )	0.00584	0.00643	0.0199	0.0566	<b>0.162</b>	0.430	0.648	
$\rho_M$ (fm $^{-3}$ )	0.0557	0.0587	0.103	0.183	<b>0.361</b>	0.871	1.59	
$\rho_\pi$ (fm $^{-3}$ )	0.0429	0.0451	0.0758	0.131	<b>0.257</b>	0.646	1.24	
$\epsilon$ (MeV/fm $^3$ )	28.1	29.8	54.4	102	<b>206</b>	444	687	
$P$ (MeV/fm $^3$ )	5.97	6.33	11.9	22.8	<b>48.9</b>	122	214	
$s$ (MeV/fm $^3$ )	0.307	0.322	0.539	0.922	<b>1.71</b>	3.49	5.52	

**Table 3.** Au+Au (70-80%) collision at  $\sqrt{s_{NN}} = 62.4$  GeV. Results obtained for different values of the magnetic field.

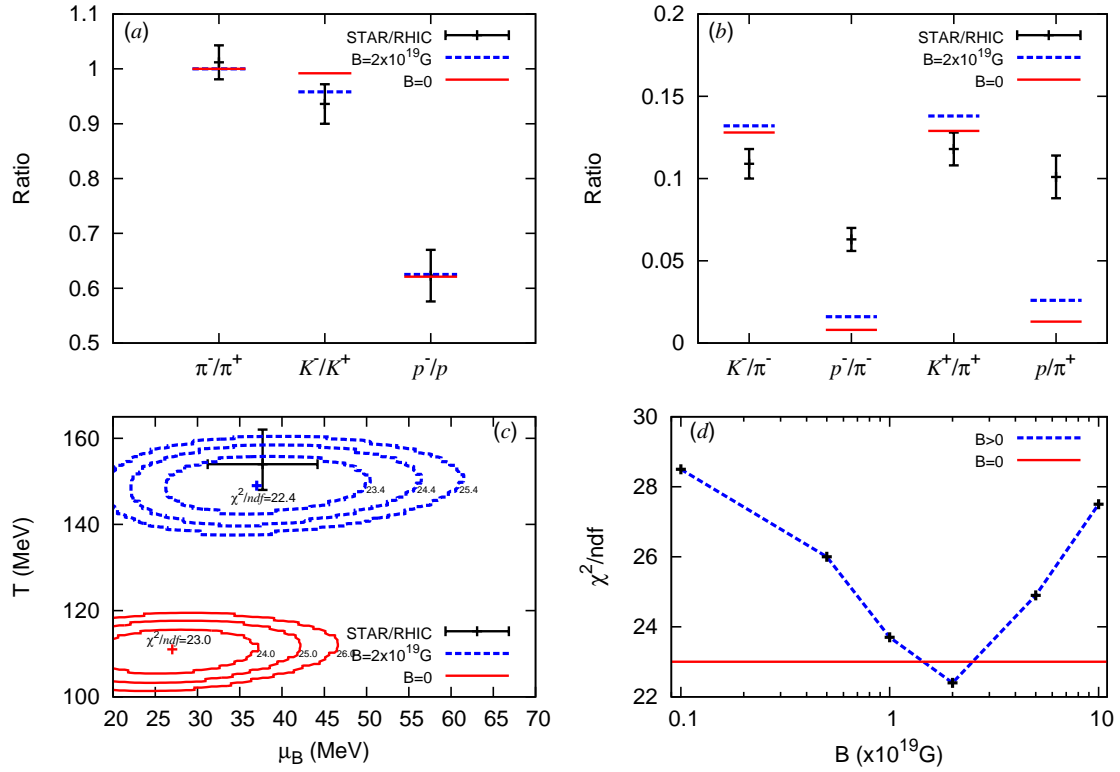


**Figure 3.** Au+Au (70-80%) collision at  $\sqrt{s_{NN}} = 62.4$  GeV. (a) particle/antiparticle ratios. (b) mixed ratios. (c) and (d)  $\chi^2$  behavior.

$B$ ( $\times 10^{19}$ G)	0	0.1	0.5	1	<b>2</b>	5	10	STAR/RHIC[30]
$eB$ ( $m_\pi^2$ )	0	0.3	1.5	3	<b>6</b>	15	30	
$\pi^-/\pi^+$ ( $\Delta\%$ )	1.000 (0.79%)	1.000	1.000	1.000	<b>1.000 (0.79%)</b>	1.000	1.000	$1.008\pm 0.042$
$K^-/K^+$	0.996 (1.98%)	0.996	0.992	0.988	<b>0.981 (0.43%)</b>	0.981	0.987	$0.977\pm 0.037$
$\bar{p}/p$	0.843 (0.18%)	0.844	0.844	0.847	<b>0.843 (0.22%)</b>	0.842	0.841	$0.841\pm 0.067$
$K^-/\pi^-$	0.137 (14.3%)	0.137	0.140	0.143	<b>0.146 (21.8%)</b>	0.146	0.142	$0.120\pm 0.011$
$\bar{p}/\pi^-$	0.011 (86.3%)	0.012	0.015	0.020	<b>0.023 (71.8%)</b>	0.019	0.014	$0.082\pm 0.010$
$K^+/\pi^+$	0.138 (11.0%)	0.138	0.141	0.145	<b>0.149 (20.1%)</b>	0.149	0.144	$0.124\pm 0.012$
$p/\pi^+$	0.013 (86.4%)	0.014	0.018	0.024	<b>0.027 (71.0%)</b>	0.023	0.017	$0.098\pm 0.014$
$T$ (MeV)	114	115	126	139	<b>155</b>	170	171	$159_{-7}^{+10}$
$\mu_B$ (MeV)	10	10	11	12	<b>14</b>	16	17	$16.5\pm 6.5$
$\mu_S$ (MeV)	0.443	0.464	0.807	1.32	<b>2.18</b>	3.00	3.26	
$\mu_{I3}$ (MeV)	-0.467	-0.475	-0.671	-0.939	<b>-1.49</b>	-2.80	-4.33	
$\chi^2/ndf$	18.2	22.5	20.5	18.6	<b>17.5</b>	19.4	21.7	
$R$ (fm)	71.5	69.5	50.2	36.4	<b>25.6</b>	18.9	17.1	
$\rho_B$ ( $\times 10^{-2}$ fm $^{-3}$ )	0.0130	0.0141	0.0375	0.0982	<b>0.283</b>	0.700	0.944	
$\rho_\Delta$ ( $\times 10^{-2}$ fm $^{-3}$ )	0.00292	0.00320	0.00936	0.0270	<b>0.0859</b>	0.237	0.344	
$\rho_M$ (fm $^{-3}$ )	0.0627	0.0660	0.113	0.204	<b>0.415</b>	1.00	1.80	
$\rho_\pi$ (fm $^{-3}$ )	0.0472	0.0495	0.0818	0.142	<b>0.283</b>	0.715	1.36	
$\epsilon$ (MeV/fm $^3$ )	33.0	34.9	62.9	121	<b>259</b>	573	857	
$P$ (MeV/fm $^3$ )	6.93	7.33	13.5	26.6	<b>59.6</b>	151	258	
$s$ (MeV/fm $^3$ )	0.350	0.367	0.606	1.06	<b>2.06</b>	4.25	6.52	

**Table 4.**  $d+\text{Au}$  (40-100%) collision at  $\sqrt{s_{NN}} = 200$  GeV. Results obtained for different values of the magnetic field.

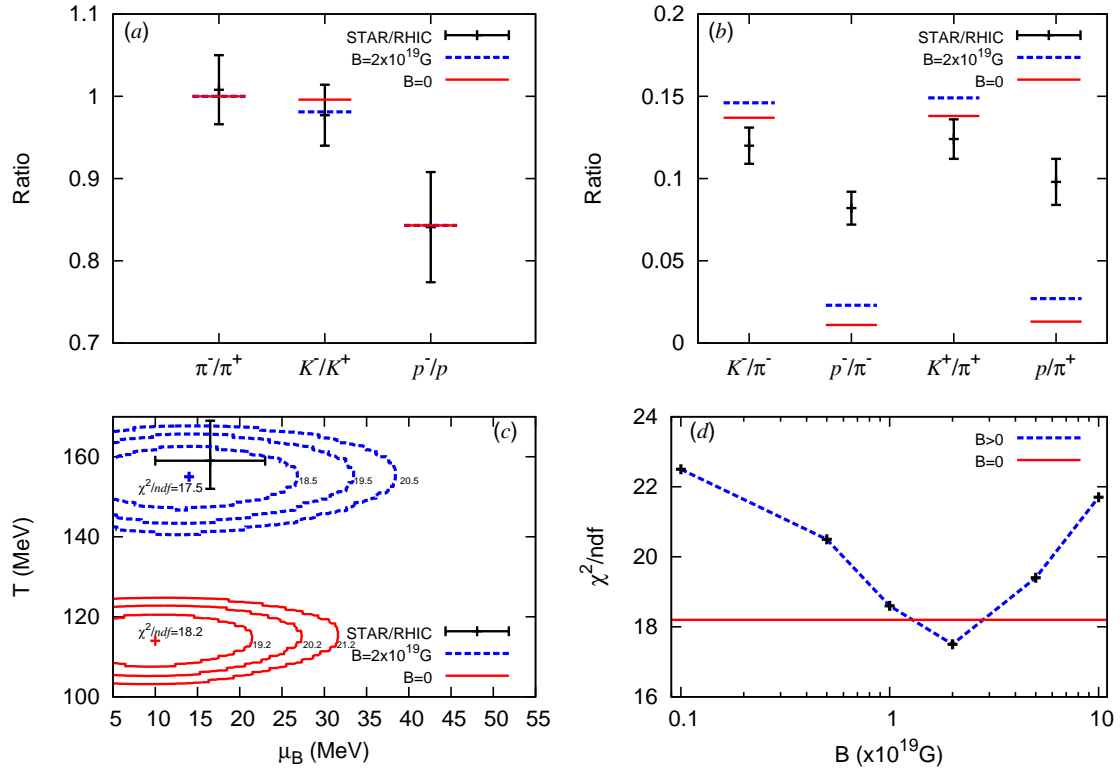


**Figure 4.**  $d+Au$  (40-100%) collision at  $\sqrt{s_{NN}} = 200$  GeV. (a) particle/antiparticle ratios. (b) mixed ratios. (c) and (d)  $\chi^2$  behavior.